

Fermi surface reconstruction in strained $\text{La}_3\text{Ni}_2\text{O}_7$ on $\text{LaAlO}_3(001)$ and $\text{SrTiO}_3(001)$

Benjamin Geisler,^{1,2,*} James J. Hamlin,¹ Gregory R. Stewart,¹ Richard G. Hennig,^{2,3} and P.J. Hirschfeld¹

¹Department of Physics, University of Florida, Gainesville, Florida 32611, USA

²Department of Materials Science and Engineering, University of Florida, Gainesville, Florida 32611, USA

³Quantum Theory Project, University of Florida, Gainesville, Florida 32611, USA

(Dated: November 25, 2024)

We explore the structural and electronic properties of the bilayer nickelate $\text{La}_3\text{Ni}_2\text{O}_7$ on $\text{LaAlO}_3(001)$ and $\text{SrTiO}_3(001)$ by using density functional theory including a Coulomb repulsion term. For $\text{La}_3\text{Ni}_2\text{O}_7/\text{LaAlO}_3(001)$, we find that compressive strain and electron doping across the interface result in the unconventional occupation of the antibonding Ni $3d_{z^2}$ states. In sharp contrast, no charge transfer is observed for $\text{La}_3\text{Ni}_2\text{O}_7/\text{SrTiO}_3(001)$. Surprisingly, tensile strain drives a metallization of the bonding Ni $3d_{z^2}$ states, rendering a Fermi surface topology resembling the superconducting bulk $\text{La}_3\text{Ni}_2\text{O}_7$ under high pressure. Concomitantly, significant octahedral rotations are retained. We discuss the fundamental differences between hydrostatic pressure and epitaxial strain regarding the crystal geometry and Ni $3d$ orbital occupation, and establish that strain provides a much stronger control over the Ni e_g orbital polarization. The results suggest epitaxial $\text{La}_3\text{Ni}_2\text{O}_7$ under tensile strain as interesting system to provide novel insights into the physics of bilayer nickelates and possibly induce superconductivity without external pressure.

Introduction. – The recent discovery of superconductivity with $T_c \sim 80$ K in pressurized $\text{La}_3\text{Ni}_2\text{O}_7$ [1–3] positioned the bilayer Ruddlesden-Popper compounds as an exciting new addition to the expanding class of superconducting nickelates, drawing significant attention [4–38]. $\text{La}_3\text{Ni}_2\text{O}_7$ is particularly intriguing as it exhibits superconductivity in bulk crystals, in contrast to infinite-layer nickelates [39–47]. The pairing mechanism has been suggested to be related to a pressure-driven change in Fermi surface topology [1, 4–6, 16] and a concomitant structural transition from an orthorhombic $Cmcm$ to a tetragonal $I4/mmm$ phase [24, 30] involving a suppression of the NiO_6 octahedral rotations [1, 16, 24, 30]. Despite strong efforts, sample growth and characterization under high pressure remain challenging, particularly in verifying the Meissner effect and detecting thermodynamic transitions.

It is therefore essential to assess alternative pathways to drive superconductivity in bilayer nickelates. Here we investigate the impact of epitaxial strain as well as electrostatic doping exploiting interface polarity. To this end, we explore the structural and electronic properties of $\text{La}_3\text{Ni}_2\text{O}_7$ on $\text{LaAlO}_3(001)$ (LAO) and $\text{SrTiO}_3(001)$ (STO) by using density functional theory including a Coulomb repulsion term, treating the interface explicitly. We identify the fundamental differences between hydrostatic pressure and biaxial strain, and show that they probe orthogonal domains in crystal geometry and Ni $3d$ orbital occupation. For $\text{La}_3\text{Ni}_2\text{O}_7/\text{LAO}(001)$, compressive strain results in the unconventional occupation of the antibonding Ni $3d_{z^2}$ states, which we find to be further promoted by electron doping across the interface. In sharp contrast, no charge transfer is observed for $\text{La}_3\text{Ni}_2\text{O}_7/\text{STO}(001)$. The Fermi energy is located in the substrate band gap in both systems, such that the active states arise exclusively from the Ni e_g orbitals. Counter-intuitively, we find that tensile epitaxial strain in $\text{La}_3\text{Ni}_2\text{O}_7/\text{STO}(001)$ renders a Fermi surface topology comparable to bulk $\text{La}_3\text{Ni}_2\text{O}_7$ under external pressure, characterized by the emergence of a Ni $3d_{z^2}$ hole pocket. Simultaneously, the octahedral rotations are preserved. These

findings suggest bilayer nickelates subject to tensile strain as an interesting platform to gain deeper insights into the pairing mechanism and as potential candidate to engineer superconductivity at ambient pressure.

Methods. – We performed density functional theory calculations [48] (DFT) by using Quantum ESPRESSO [49] in conjunction with the exchange-correlation functional by Perdew, Burke, and Ernzerhof [50] and ultrasoft pseudopotentials [51], as successfully employed in previous work [52–54]. Static correlation effects were considered within DFT+ U [55] employing $U = 4$ eV on Ni and Ti sites [1, 16, 56–58]. To accurately describe the octahedral rotations, we use $\sqrt{2}a \times \sqrt{2}a \times c$ supercells with two transition metal sites per layer, setting a to the substrate lattice parameter ($a_{\text{LAO}} = 3.79$ Å, $a_{\text{STO}} = 3.905$ Å) and optimizing c . The symmetric supercells contain two equivalent interfaces, 3 bilayers of $\text{La}_3\text{Ni}_2\text{O}_7$ (LNO), and 6.5 layers of substrate, corresponding to 136 atoms in the unit cell (Fig. 1). Wave functions and density were expanded into plane waves up to cutoff energies of 35 and 350 Ry, respectively. The Brillouin zone was sampled by using a $12 \times 12 \times 1$ Monkhorst-Pack \vec{k} -point grid [59] and 5 mRy Methfessel-Paxton smearing [60]. The ionic positions were accurately optimized, reducing ionic forces below 1 mRy/a.u. Subsequently, Fermi surfaces and densities of states were obtained by using $64 \times 64 \times 4$ \vec{k} -point grids. Reference calculations for bulk LNO at 0 GPa ($Cmcm$) and 30 GPa ($I4/mmm$) were performed by using 48-atom supercells [24, 34] with $12 \times 12 \times 4$ and $64 \times 64 \times 8$ \vec{k} -point grids. Tight-binding Hamiltonians describing the Ni electronic structure in a basis of maximally localized Wannier functions [61] are provided in the Supplemental Information (SI) [62].

Ionic relaxation, electronic structure, and interfacial charge transfer. – Figure 1(a,b) shows the optimized geometry and layer-resolved density of states of epitaxial $\text{La}_3\text{Ni}_2\text{O}_7$ on $\text{LaAlO}_3(001)$ and $\text{SrTiO}_3(001)$. These prototypical substrates exert compressive and tensile strain on the bilayer nickelate (pseudocubic $a_{\text{LNO}} = 3.83$ Å), respectively. The optimized

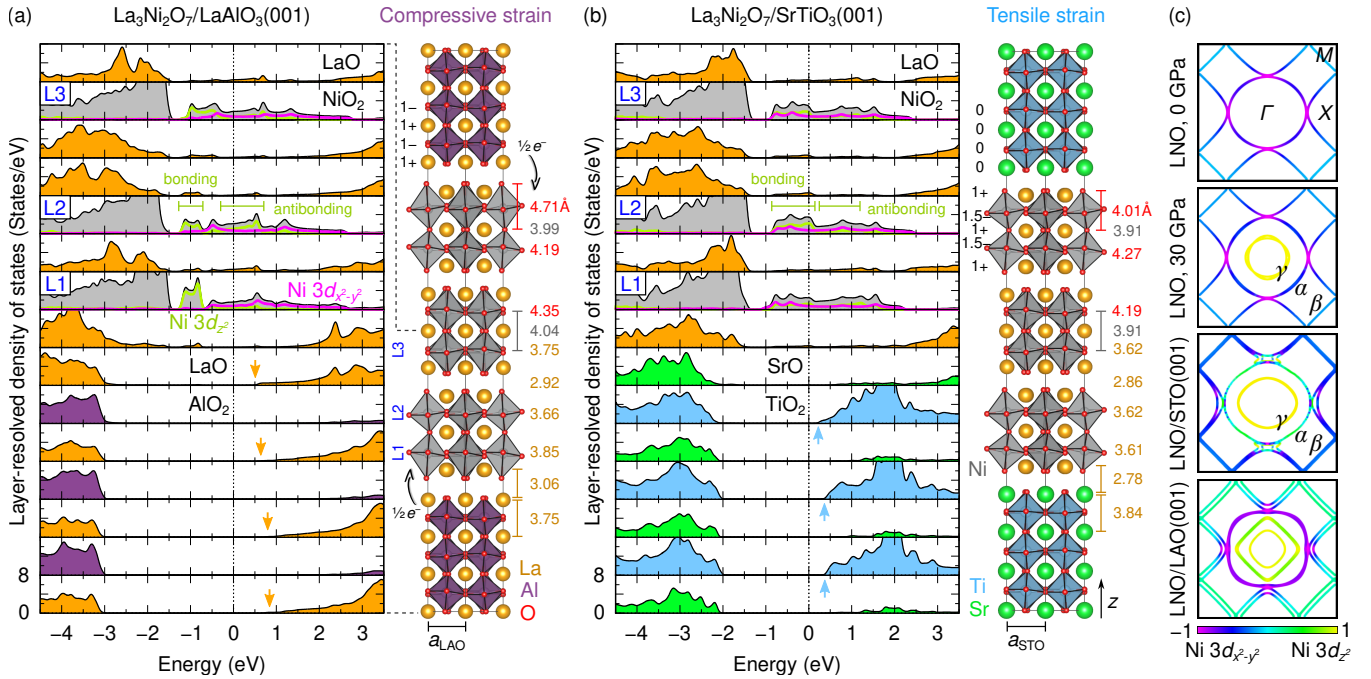


Figure 1. **Optimized geometry, electronic structure, and Fermi surfaces of the bilayer nickelate systems considered here.** (a,b) Optimized geometry and layer-resolved density of states of $\text{La}_3\text{Ni}_2\text{O}_7$ (LNO) on LAO(001) (compressive strain) and STO(001) (tensile strain). The numbers on the right of each structure denote the A - (orange) and Ni-site distances (grey) as well as the O-Ni-O bond lengths (red) in z direction. The formal layer polarity is given by the black numbers. Both substrates show no involvement in the Fermi surface, although a downwards bending of their conduction-band states near the interface can be observed (orange and blue arrows). (c) Fermi surfaces, colored by the Ni orbital character $(3d_{z^2} - 3d_{x^2-y^2})/(3d_{z^2} + 3d_{x^2-y^2})$. The orbital character of the α and β sheets is considerably modulated by strain, exceeding the effect of external pressure. On LAO, the central pockets stem from the antibonding Ni $3d_{z^2}$ states due to a concerted effect of compressive strain and charge transfer across the interface. In sharp contrast, the STO substrate drives a metallization of the bonding Ni $3d_{z^2}$ states (γ), resembling pressurized bulk $\text{La}_3\text{Ni}_2\text{O}_7$.

height of the nickelate region, defined as the distance between the two interfaces, corresponds to $3/2 \cdot c_{\text{LNO}}$ of an orthorhombic $\text{La}_3\text{Ni}_2\text{O}_7$ reference cell, yielding $c_{\text{LNO}} = 20.13 \text{ \AA}$ on STO and 20.95 \AA on LAO. Compared to the bulk lattice parameter of 20.6 \AA [24], the structure on STO (LAO) is thus considerably contracted (expanded) due to strain effects.

This trend is also evident in the vertical A - and Ni-site distances [Fig. 1(a,b)], which can directly be measured by using transmission electron microscopy. The A -site distances in the bilayers remain nearly constant at $\sim 3.62 \text{ \AA}$ on STO, a notable reduction compared to the bulk value of 3.70 \AA . In contrast, these distances vary from 3.66 to 3.85 \AA on LAO. Across the structural gap between the bilayers, we find A -site distances of 2.86 \AA on STO and 2.92 \AA on LAO, compared to the bulk value of 2.90 \AA . For the Ni sites, the bulk separation of 3.94 \AA contracts to 3.91 \AA on STO and expands to 3.99 \AA – 4.04 \AA on LAO. These observations highlight that the interlayer coupling between the Ni sites can be modulated by epitaxial strain.

The interface geometry considered here [Fig. 1(a,b)] represents a natural continuation of the two constituent structures and resembles the layer stacking of related Ruddlesden-Popper cuprate-perovskite nickelate systems successfully

grown in a previous study [53]. In [001] direction, each bilayer of the nickelate consists of three $(\text{LaO})^{1+}$ and two $(\text{NiO}_2)^{1.5-}$ layers yielding a nominal Ni $3d^{7.5}$ valence. In contrast, STO is composed of charge-neutral $(\text{SrO})^0$ and $(\text{TiO}_2)^0$ layers, while LAO presents an alternating formal layer polarity of $(\text{LaO})^{1+}$ and $(\text{AlO}_2)^{1-}$. This raises an intriguing question about how the different polar discontinuities at the interfaces to the two band insulators are accommodated.

The layer-resolved densities of states in Fig. 1(a,b) reflect the relative band alignment of the constituent oxides. We find in both systems that the Fermi energy is clearly located in the substrate band gap. Therefore, the Fermi surfaces in Fig. 1(c) are exclusively formed by the Ni e_g states, although both substrates exhibit a clear lowering of the conduction-band states towards the interface [marked by orange and blue arrows in Fig. 1(a,b)]. Specifically, in the STO system, the conduction band edge of the substrate is identified $\sim 250 \text{ meV}$ above the Fermi level, and no correlated two-dimensional electron gas (2DEG) forms at the interface. This constitutes a fundamental difference to infinite-layer nickelate films on STO(001) with ideal interface geometry [56, 57, 63, 64].

In the LAO system, we find that the polar interface dopes half an electron per unit area, which is accommodated in

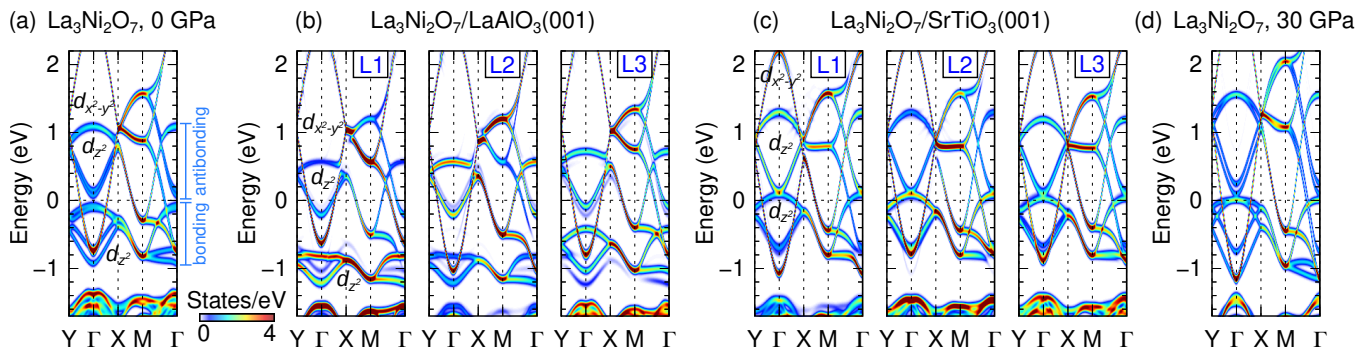


Figure 2. **Projected band structure of the four considered bilayer nickelate systems.** Momentum-resolved density of states, projected on the Ni $3d$ orbitals in layers L1-L3 of (b) $\text{La}_3\text{Ni}_2\text{O}_7/\text{LAO}(001)$ and (c) $\text{La}_3\text{Ni}_2\text{O}_7/\text{STO}(001)$ (cf. Fig. 1). For comparison, consistently obtained bulk Ni $3d$ bands at (a) 0 and (d) 30 GPa are shown. Remarkable are the distinct response of the Ni e_g bands to hydrostatic pressure versus epitaxial strain, as well as the occupation (depletion) of the (anti)bonding Ni $3d_{z^2}$ states on LAO (STO) at the Γ point (see also SI).

$\text{La}_3\text{Ni}_2\text{O}_7$ due to the wide band gap of LAO [Fig. 1(a)]. Hence, the superconductor is charge doped without the need for chemical doping. Tuning the thickness of the nickelate region may be an attractive route to control the density of the doped charge in the NiO_2 planes. At the interface, we observe an expanded A -site distance of 3.06 \AA relative to the bulk. This expansion is attributed to the electrostatic doping and closely resembles the enhanced La-Sr and Nd-Sr distances across n -type interfaces in perovskite $\text{LaNiO}_3/\text{STO}(001)$ [65–67] and infinite-layer $\text{NdNiO}_2/\text{STO}(001)$ [56]. Conversely, in the STO system, the corresponding A -site distance is significantly smaller (2.78 \AA), which is a manifestation of the non-polar substrate [Fig. 1(b)].

The O-Ni-O bond lengths are closely linked to the relative energies and occupation of the Ni e_g orbitals and exhibit a significant response to the different substrates (Fig. 1). On LAO, we identify a general elongation in z direction, reaching up to 4.71 \AA , while on STO, they are contracted to as short as 4.01 \AA , both relative to the bulk value of 4.27 \AA . Conversely, the in-plane O-Ni-O bond lengths amount to 3.81 \AA on LAO and 3.93 \AA on STO, with a bulk value of 3.85 \AA .

The overall expanded vertical bond lengths on LAO lower the energy of the Ni $3d_{z^2}$ orbital relative to Ni $3d_{x^2-y^2}$, as evidenced by the projected momentum-resolved density of states, $A_i(\epsilon, k) = \sum_n \langle \phi_i | \psi_{n,k} \rangle \delta(\epsilon_{n,k} - \epsilon)$, where ϕ_i denotes Ni $3d$ manifolds at different sites i . We find that this results in the unconventional occupation of the antibonding Ni $3d_{z^2}$ states around the Γ point [Fig 2(b)], which are completely empty in the bulk, even under finite pressure [Fig 2(a,d)]. This phenomenon is further promoted by the doped charge. Simultaneously, the bonding Ni $3d_{z^2}$ states are completely filled. In layer L1, they are lowered to $\sim -1 \text{ eV}$ and present a considerably reduced bandwidth [Figs. 1(a), 2(b)], which coincides with a strong elongation of the corresponding NiO_6 octahedra. In layer L3, these states appear at slightly higher energies and with enhanced band width, yet still $\sim 0.4 \text{ eV}$ below the Fermi level.

Intriguingly, the opposite trend is observed for the STO sys-

tem, in which the bonding Ni $3d_{z^2}$ states form flat bands near the Fermi level and are partially depleted, similar to pressurized bulk $\text{La}_3\text{Ni}_2\text{O}_7$ [Fig 2(c)]. No interfacial charge transfer occurs, and their energies and band widths remain rather constant throughout all layers.

Fermi surface reconstruction. – The contrasting response of the electronic structure to compressive versus tensile strain results in fundamentally distinct Fermi surfaces [Fig. 1(c)]. Previous work identified the characteristic Fermi surface of $\text{La}_3\text{Ni}_2\text{O}_7$ to be composed of two sheets: One of predominantly Ni $3d_{x^2-y^2}$ character (α), and one with some admixture of Ni $3d_{z^2}$ (β) [4–6, 27]. Upon application of hydrostatic pressure, the Fermi surface undergoes a topological transition, resulting in the emergence of a hole pocket of strong Ni $3d_{z^2}$ character (γ) [1, 4–7, 16, 21].

In the STO system, we find significant enhancements of both the Ni $3d_{z^2}$ contribution to the α sheet, as well as the Ni $3d_{x^2-y^2}$ character of the β sheet [Fig. 1(c)]. Most importantly, the metallization of the bonding Ni $3d_{z^2}$ states results in a Fermi surface topology comparable to the high- T_c superconductor $\text{La}_3\text{Ni}_2\text{O}_7$ under external pressure, characterized by the emergence of a γ hole pocket. We speculate that the size of the pocket can be controlled by strain tuning.

In sharp contrast, the LAO substrate results in a splitting (broadening) of the β sheet due to electrostatic doping and interfacial symmetry breaking, accompanied by an enhanced Ni $3d_{z^2}$ contribution. The α sheet appears considerably more rectangular than in the bulk and displays an enhanced Ni $3d_{x^2-y^2}$ character. Additional sheets can be identified around the Γ point, which stem from the antibonding Ni $3d_{z^2}$ states, distinct from the STO case. The overall shape of the Fermi surface suggests the potential for strong nesting.

These findings establish that epitaxial strain and interface polarity provide substantial control over the Fermi surface topology that exceed even the effect of external pressure. It is reasonable to assume that this will considerably impact the superconducting pairing in the nickelate. Particularly tensile strain emerges as promising strategy to induce ambient-

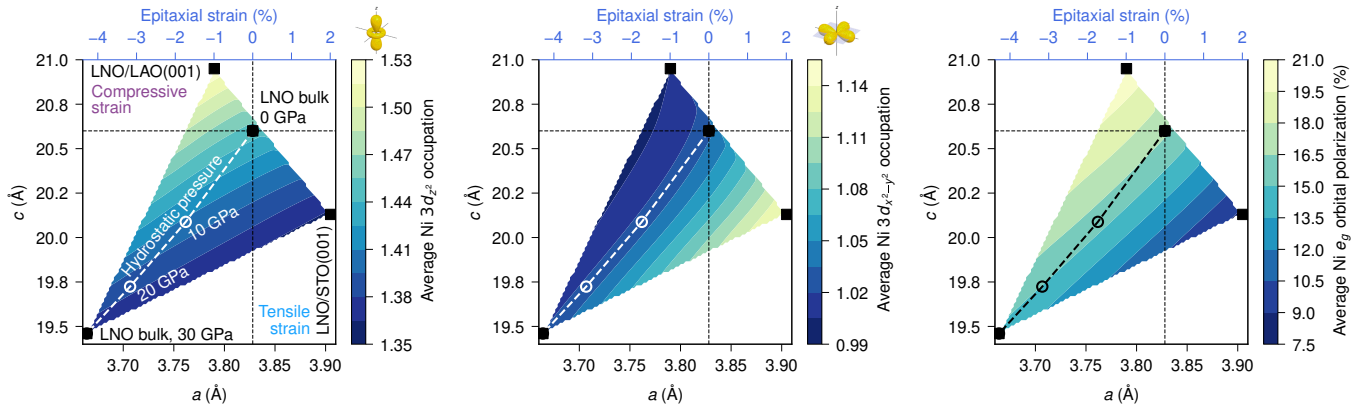


Figure 3. Fundamental difference between hydrostatic pressure and epitaxial strain in bilayer nickelates. The panels show the correlations between the optimized lattice parameters and the Ni $3d$ orbital occupation for bulk $\text{La}_3\text{Ni}_2\text{O}_7$ (LNO) at 0 GPa, 30 GPa, LNO/LAO(001), and LNO/STO(001) (black squares). For the latter two systems, a is fixed by the substrate, which exerts the epitaxial strain $\varepsilon = a/a_{\text{LNO}} - 1$ on the nickelate. The dashed line connects the reference points obtained under hydrostatic pressure, which we find to explore structural and electronic domains of bilayer nickelates that are orthogonal to those accessible under epitaxial strain. The colors represent (from left to right) the average occupation of Ni $3d_{z^2}$, Ni $3d_{x^2-y^2}$, and the resulting Ni e_g orbital polarization, interpolated between the exact data points to emphasize the trends. This highlights that epitaxial strain provides a much stronger control over the orbital polarization than external pressure.

pressure superconductivity in $\text{La}_3\text{Ni}_2\text{O}_7$ due to the strong coupling of the α and β sheets with the emerging γ pocket and calls for further investigation. Notably, the Fermi surface reconstruction is not accompanied by a suppression of the NiO_6 octahedral rotations [Fig. 1(a,b)], not even under compressive strain. This marks an important difference to pressurized bulk $\text{La}_3\text{Ni}_2\text{O}_7$ [1, 16, 24, 30]. We conclude that it is possible to tune the electronic structure of the nickelate independently of the octahedral degrees of freedom, which grants access to a deeper understanding of the mechanisms leading to superconductivity in bilayer nickelates.

Fundamental differences between hydrostatic pressure and epitaxial strain. – The essence of these results is compiled in Fig. 3, which establishes the key differences between hydrostatic pressure and epitaxial strain in bilayer nickelates. The panels show the correlations between the optimized lattice parameters and the average occupation of the Ni $3d$ orbitals for bulk $\text{La}_3\text{Ni}_2\text{O}_7$ at 0 GPa, 30 GPa, $\text{La}_3\text{Ni}_2\text{O}_7/\text{LAO}(001)$, and $\text{La}_3\text{Ni}_2\text{O}_7/\text{STO}(001)$. In the case of orthorhombic bulk $\text{La}_3\text{Ni}_2\text{O}_7$, we show the pseudocubic a value. For the heterostructures, a is fixed by the substrate, and we show the optimized c_{LNO} value determined as described above.

Interestingly, we find that epitaxial strain explores structural and electronic domains of the bilayer nickelates that are orthogonal to those accessible under external pressure. Hydrostatic pressure results in the simultaneous compression of a and c , corresponding to the lower-left quadrant in each panel of Fig. 3. This reduces the Ni $3d_{z^2}$ occupation from 1.45 (0 GPa) to 1.37 (30 GPa), while maintaining an approximately constant Ni $3d_{x^2-y^2}$ occupation (~ 1.03). In sharp contrast, epitaxial strain leads to an opposite evolution of a and c , represented by the upper-left and lower-right quadrants in Fig. 3, which drives a significant charge transfer from Ni $3d_{z^2}$ to

Ni $3d_{x^2-y^2}$ for tensile strain, and vice versa for compressive strain. This allows to control the Ni e_g orbital polarization $(3d_{z^2} - 3d_{x^2-y^2})/(3d_{z^2} + 3d_{x^2-y^2})$ [54] over a considerably larger interval than hydrostatic pressure. Here, we find it to range from $\sim 8\%$ on STO to $\sim 21\%$ on LAO (Fig. 3).

Simultaneously, Fig. 3 compares the characteristic length scales accessible in the different experimental techniques. We see that the values for a (c) obtained due to epitaxial strain on LAO (STO) require ~ 10 GPa external pressure. On the other hand, application of 30 GPa results in a contraction of the basal lattice parameters corresponding to $\sim 4\%$ compressive strain, which is readily achievable in experiment. This highlights the scope of the different strategies to alter the crystal geometry and thereby the quantum phase of bilayer nickelates.

Summary. – We investigated the impact of epitaxial strain and interface polarity in $\text{La}_3\text{Ni}_2\text{O}_7$ on $\text{LaAlO}_3(001)$ and $\text{SrTiO}_3(001)$ by performing first-principles simulations including a Coulomb repulsion term. For $\text{La}_3\text{Ni}_2\text{O}_7/\text{LaAlO}_3(001)$, compressive strain in conjunction with electron doping across the explicitly treated interface results in the unconventional occupation of the antibonding Ni $3d_{z^2}$ states. In sharp contrast, no charge transfer was observed for $\text{La}_3\text{Ni}_2\text{O}_7/\text{SrTiO}_3(001)$. Intriguingly, tensile strain was found to drive a metallization of the bonding Ni $3d_{z^2}$ states in this system that yields a Fermi surface topology resembling bulk $\text{La}_3\text{Ni}_2\text{O}_7$ under high pressure. We demonstrated that such transitions in the electronic structure, considered to be key for high- T_c superconductivity in bilayer nickelates, are decoupled from quenching the octahedral rotations. In addition, we identified the fundamental differences between hydrostatic pressure and epitaxial strain regarding the crystal geometry and Ni $3d$ orbital occupation, and established that strain provides a much stronger control over the Ni e_g or-

bital polarization.

The great promise of high- T_c nickelate superconductivity will only be realized if structures favorable for electron pairing can be created at ambient pressure. Our results show that epitaxial strain is an excellent avenue to explore in this direction. Already moderate strain as exerted by the technologically relevant substrates LaAlO_3 and SrTiO_3 is predicted to alter the electronic properties considerably due to the strong response of the Ni orbitals. We particularly emphasized the similarity of $\text{La}_3\text{Ni}_2\text{O}_7$ under tensile strain to the high- T_c pressurized bulk compound, suggesting the potential for superconductivity at ambient pressure. Finally, the proposed strategy avoids chemical doping and concomitant disorder, and may hence allow even higher critical temperatures than heretofore achieved.

Acknowledgments. – This work was supported by the National Science Foundation, Grant No. NSF-DMR-2118718.

* benjamin.geisler@ufl.edu

- [1] H. Sun, M. Huo, X. Hu, J. Li, Z. Liu, Y. Han, L. Tang, Z. Mao, P. Yang, B. Wang, J. Cheng, D.-X. Yao, G.-M. Zhang, and M. Wang, Signatures of superconductivity near 80 K in a nickelate under high pressure, *Nature* **621**, 493 (2023).
- [2] J. Hou, P.-T. Yang, Z.-Y. Liu, J.-Y. Li, P.-F. Shan, L. Ma, G. Wang, N.-N. Wang, H.-Z. Guo, J.-P. Sun, Y. Uwatoko, M. Wang, G.-M. Zhang, B.-S. Wang, and J.-G. Cheng, Emergence of high-temperature superconducting phase in pressurized $\text{La}_3\text{Ni}_2\text{O}_7$ crystals, *Chin. Phys. Lett.* **40**, 117302 (2023).
- [3] Y. Zhang, D. Su, Y. Huang, Z. Shan, H. Sun, M. Huo, K. Ye, J. Zhang, Z. Yang, Y. Xu, Y. Su, R. Li, M. Smidman, M. Wang, L. Jiao, and H. Yuan, High-temperature superconductivity with zero resistance and strange-metal behaviour in $\text{La}_3\text{Ni}_2\text{O}_{7-\delta}$, *Nature Physics* **20**, 1269 (2024).
- [4] Z. Luo, X. Hu, M. Wang, W. Wú, and D.-X. Yao, Bilayer two-orbital model of $\text{La}_3\text{Ni}_2\text{O}_7$ under pressure, *Phys. Rev. Lett.* **131**, 126001 (2023).
- [5] Y. Gu, C. Le, Z. Yang, X. Wu, and J. Hu, Effective model and pairing tendency in bilayer Ni-based superconductor $\text{La}_3\text{Ni}_2\text{O}_7$ (2023), [arXiv:2306.07275 \[cond-mat.supr-con\]](https://arxiv.org/abs/2306.07275).
- [6] Q.-G. Yang, D. Wang, and Q.-H. Wang, Possible s_{\pm} -wave superconductivity in $\text{La}_3\text{Ni}_2\text{O}_7$, *Phys. Rev. B* **108**, L140505 (2023).
- [7] F. Lechermann, J. Gondolf, S. Bötzel, and I. M. Eremin, Electronic correlations and superconducting instability in $\text{La}_3\text{Ni}_2\text{O}_7$ under high pressure, *Phys. Rev. B* **108**, L201121 (2023).
- [8] H. Sakakibara, N. Kitamine, M. Ochi, and K. Kuroki, Possible high T_c superconductivity in $\text{La}_3\text{Ni}_2\text{O}_7$ under high pressure through manifestation of a nearly half-filled bilayer Hubbard model, *Phys. Rev. Lett.* **132**, 106002 (2024).
- [9] Y. Shen, M. Qin, and G.-M. Zhang, Effective bi-layer model hamiltonian and density-matrix renormalization group study for the high- T_c superconductivity in $\text{La}_3\text{Ni}_2\text{O}_7$ under high pressure, *Chin. Phys. Lett.* **40**, 127401 (2023).
- [10] V. Christiansson, F. Petocchi, and P. Werner, Correlated electronic structure of $\text{La}_3\text{Ni}_2\text{O}_7$ under pressure, *Phys. Rev. Lett.* **131**, 206501 (2023).
- [11] D. A. Shilenko and I. V. Leonov, Correlated electronic structure, orbital-selective behavior, and magnetic correlations in double-layer $\text{La}_3\text{Ni}_2\text{O}_7$ under pressure, *Phys. Rev. B* **108**, 125105 (2023).
- [12] W. Wú, Z. Luo, D.-X. Yao, and M. Wang, Superexchange and charge transfer in the nickelate superconductor $\text{La}_3\text{Ni}_2\text{O}_7$ under pressure, *Science China Physics, Mechanics & Astronomy* **67**, 117402 (2024).
- [13] Y. Cao and Y.-f. Yang, Flat bands promoted by Hund's rule coupling in the candidate double-layer high-temperature superconductor $\text{La}_3\text{Ni}_2\text{O}_7$ under high pressure, *Phys. Rev. B* **109**, L081105 (2024).
- [14] X. Chen, P. Jiang, J. Li, Z. Zhong, and Y. Lu, Critical charge and spin instabilities in superconducting $\text{La}_3\text{Ni}_2\text{O}_7$ (2023), [arXiv:2307.07154 \[cond-mat.supr-con\]](https://arxiv.org/abs/2307.07154).
- [15] C. Lu, Z. Pan, F. Yang, and C. Wu, Interlayer-coupling-driven high-temperature superconductivity in $\text{La}_3\text{Ni}_2\text{O}_7$ under pressure, *Phys. Rev. Lett.* **132**, 146002 (2024).
- [16] Y. Zhang, L.-F. Lin, A. Moreo, T. A. Maier, and E. Dagotto, Structural phase transition, s_{\pm} -wave pairing, and magnetic stripe order in bilayered superconductor $\text{La}_3\text{Ni}_2\text{O}_7$ under pressure, *Nat. Commun.* **15**, 2470 (2024).
- [17] Z. Liao, L. Chen, G. Duan, Y. Wang, C. Liu, R. Yu, and Q. Si, Electron correlations and superconductivity in $\text{La}_3\text{Ni}_2\text{O}_7$ under pressure tuning (2023), [arXiv:2307.16697 \[cond-mat.supr-con\]](https://arxiv.org/abs/2307.16697).
- [18] X.-Z. Qu, D.-W. Qu, J. Chen, C. Wu, F. Yang, W. Li, and G. Su, Bilayer t - j - j_{\perp} model and magnetically mediated pairing in the pressurized nickelate $\text{La}_3\text{Ni}_2\text{O}_7$, *Phys. Rev. Lett.* **132**, 036502 (2024).
- [19] J. Huang, Z. D. Wang, and T. Zhou, Impurity and vortex states in the bilayer high-temperature superconductor $\text{La}_3\text{Ni}_2\text{O}_7$, *Phys. Rev. B* **108**, 174501 (2023).
- [20] Q. Qin and Y.-f. Yang, High- T_c superconductivity by mobilizing local spin singlets and possible route to higher T_c in pressurized $\text{La}_3\text{Ni}_2\text{O}_7$, *Phys. Rev. B* **108**, L140504 (2023).
- [21] Y.-B. Liu, J.-W. Mei, F. Ye, W.-Q. Chen, and F. Yang, s_{\pm} -wave pairing and the destructive role of apical-oxygen deficiencies in $\text{La}_3\text{Ni}_2\text{O}_7$ under pressure, *Phys. Rev. Lett.* **131**, 236002 (2023).
- [22] Y. Zhang, L.-F. Lin, A. Moreo, T. A. Maier, and E. Dagotto, Trends in electronic structures and possible s_{\pm} -wave pairing for the rare-earth series in bilayer nickelate superconductor $R_3\text{Ni}_2\text{O}_7$, *Phys. Rev. B* **108**, 165141 (2023).
- [23] Z. Liu, M. Huo, J. Li, Q. Li, Y. Liu, Y. Dai, X. Zhou, J. Hao, Y. Lu, M. Wang, and H.-H. Wen, Electronic correlations and partial gap in the bilayer nickelate $\text{La}_3\text{Ni}_2\text{O}_7$, *Nat. Commun.* **15**, 7570 (2024).
- [24] B. Geisler, J. J. Hamlin, G. R. Stewart, R. G. Hennig, and P. J. Hirschfeld, Structural transitions, octahedral rotations, and electronic properties of $A_3\text{Ni}_2\text{O}_7$ rare-earth nickelates under high pressure, *npj Quantum Materials* **9**, 38 (2024).
- [25] L. C. Rhodes and P. Wahl, Structural routes to stabilize superconducting $\text{La}_3\text{Ni}_2\text{O}_7$ at ambient pressure, *Phys. Rev. Mater.* **8**, 044801 (2024).
- [26] G. Wang, N. Wang, J. Hou, L. Ma, L. Shi, Z. Ren, Y. Gu, X. Shen, H. Ma, P. Yang, Z. Liu, H. Guo, J. Sun, G. Zhang, J. Yan, B. Wang, Y. Uwatoko, and J. Cheng, Pressure-induced superconductivity in polycrystalline $\text{La}_3\text{Ni}_2\text{O}_7$ (2023), [arXiv:2309.17378 \[cond-mat.supr-con\]](https://arxiv.org/abs/2309.17378).
- [27] J. Yang, H. Sun, X. Hu, Y. Xie, T. Miao, H. Luo, H. Chen, B. Liang, W. Zhu, G. Qu, C.-Q. Chen, M. Huo, Y. Huang, S. Zhang, F. Zhang, F. Yang, Z. Wang, Q. Peng, H. Mao, G. Liu, Z. Xu, T. Qian, D.-X. Yao, M. Wang, L. Zhao, and X. J. Zhou, Orbital-dependent electron correlation in double-layer nickelate

- La₃Ni₂O₇ (2023), [arXiv:2309.01148 \[cond-mat.supr-con\]](#).
- [28] C. Lu, Z. Pan, F. Yang, and C. Wu, Interplay of two e_g orbitals in superconducting La₃Ni₂O₇ under pressure (2023), [arXiv:2310.02915 \[cond-mat.supr-con\]](#).
- [29] G. Wang, N. Wang, Y. Wang, L. Shi, X. Shen, J. Hou, H. Ma, P. Yang, Z. Liu, H. Zhang, X. Dong, J. Sun, B. Wang, K. Jiang, J. Hu, Y. Uwatoko, and J. Cheng, Observation of high-temperature superconductivity in the high-pressure tetragonal phase of La₂PrNi₂O_{7- δ} (2023), [arXiv:2311.08212 \[cond-mat.supr-con\]](#).
- [30] L. Wang, Y. Li, S. Xie, F. Liu, H. Sun, C. Huang, Y. Gao, T. Nakagawa, B. Fu, B. Dong, Z. Cao, R. Yu, S. I. Kawaguchi, H. Kadobayashi, M. Wang, C. Jin, H. Kwang Mao, and H. Liu, Structure responsible for the superconducting state in La₃Ni₂O₇ at high pressure and low temperature conditions (2023), [arXiv:2311.09186 \[cond-mat.supr-con\]](#).
- [31] K. Chen, X. Liu, J. Jiao, M. Zou, C. Jiang, X. Li, Y. Luo, Q. Wu, N. Zhang, Y. Guo, and L. Shu, Evidence of spin density waves in La₃Ni₂O_{7- δ} , *Phys. Rev. Lett.* **132**, 256503 (2024).
- [32] Y.-Y. Zheng and W. Wu, Superconductivity in the bilayer two-orbital hubbard model (2023), [arXiv:2312.03605 \[cond-mat.str-el\]](#).
- [33] M. Kakoi, T. Kaneko, H. Sakakibara, M. Ochi, and K. Kuroki, Pair correlations of the hybridized orbitals in a ladder model for the bilayer nickelate La₃Ni₂O₇ (2023), [arXiv:2312.04304 \[cond-mat.supr-con\]](#).
- [34] B. Geisler, L. Fanfarillo, J. J. Hamlin, G. R. Stewart, R. G. Hennig, and P. J. Hirschfeld, Optical properties and electronic correlations in La₃Ni₂O₇ bilayer nickelates under high pressure, *npj Quantum Materials* **9**, 89 (2024).
- [35] Z. Dong, M. Huo, J. Li, J. Li, P. Li, H. Sun, L. Gu, Y. Lu, M. Wang, Y. Wang, and Z. Chen, Visualization of oxygen vacancies and self-doped ligand holes in La₃Ni₂O_{7- δ} , *Nature* **630**, 847 (2024).
- [36] X. Chen, J. Zhang, A. S. Thind, S. Sharma, H. LaBollita, G. Peterson, H. Zheng, D. P. Phelan, A. S. Botana, R. F. Klie, and J. F. Mitchell, Polymorphism in the ruddlesden–popper nickelate La₃Ni₂O₇: Discovery of a hidden phase with distinctive layer stacking, *J. Am. Chem. Soc.* **146**, 3640 (2024).
- [37] N. Wang, G. Wang, X. Shen, J. Hou, J. Luo, X. Ma, H. Yang, L. Shi, J. Dou, J. Feng, J. Yang, Y. Shi, Z. Ren, H. Ma, P. Yang, Z. Liu, Y. Liu, H. Zhang, X. Dong, Y. Wang, K. Jiang, J. Hu, S. Nagasaki, K. Kitagawa, S. Calder, J. Yan, J. Sun, B. Wang, R. Zhou, Y. Uwatoko, and J. Cheng, Bulk high-temperature superconductivity in pressurized tetragonal La₂PrNi₂O₇, *Nature* **634**, 579 (2024).
- [38] H. LaBollita, V. Pardo, M. R. Norman, and A. S. Botana, *Assessing the formation of spin and charge stripes in La₃Ni₂O₇ from first-principles* (2024), [arXiv:2407.14409 \[cond-mat.str-el\]](#).
- [39] D. Li, K. Lee, B. Y. Wang, M. Osada, S. Crossley, H. R. Lee, Y. Cui, Y. Hikita, and H. Y. Hwang, Superconductivity in an infinite-layer nickelate, *Nature* **572**, 624 (2019).
- [40] Q. Li, C. He, J. Si, X. Zhu, Y. Zhang, and H.-H. Wen, Absence of superconductivity in bulk Nd_{1- x} Sr _{x} NiO₂, *Communications Materials* **1**, 16 (2020).
- [41] A. S. Botana and M. R. Norman, Similarities and differences between LaNiO₂ and CaCuO₂ and implications for superconductivity, *Phys. Rev. X* **10**, 011024 (2020).
- [42] D. Li, B. Y. Wang, K. Lee, S. P. Harvey, M. Osada, B. H. Goodge, L. F. Kourkoutis, and H. Y. Hwang, Superconducting dome in Nd_{1- x} Sr _{x} NiO₂ infinite layer films, *Phys. Rev. Lett.* **125**, 027001 (2020).
- [43] S. Zeng, C. S. Tang, X. Yin, C. Li, M. Li, Z. Huang, J. Hu, W. Liu, G. J. Omar, H. Jani, Z. S. Lim, K. Han, D. Wan, P. Yang, S. J. Pennycook, A. T. S. Wee, and A. Ariando, Phase diagram and superconducting dome of infinite-layer Nd_{1- x} Sr _{x} NiO₂ thin films, *Phys. Rev. Lett.* **125**, 147003 (2020).
- [44] M. Osada, B. Y. Wang, B. H. Goodge, K. Lee, H. Yoon, K. Sakuma, D. Li, M. Miura, L. F. Kourkoutis, and H. Y. Hwang, A superconducting praseodymium nickelate with infinite layer structure, *Nano Lett.* **20**, 5735 (2020).
- [45] B.-X. Wang, H. Zheng, E. Krivyakina, O. Chmaissem, P. P. Lopes, J. W. Lynn, L. C. Gallington, Y. Ren, S. Rosenkranz, J. F. Mitchell, and D. Phelan, Synthesis and characterization of bulk Nd_{1- x} Sr _{x} NiO₂ and Nd_{1- x} Sr _{x} NiO₃, *Phys. Rev. Materials* **4**, 084409 (2020).
- [46] M. Osada, B. Y. Wang, B. H. Goodge, S. P. Harvey, K. Lee, D. Li, L. F. Kourkoutis, and H. Y. Hwang, Nickelate superconductivity without rare-earth magnetism: (La,Sr)NiO₂, *Adv. Mater.* **33**, 2104083 (2021).
- [47] B. H. Goodge, B. Geisler, K. Lee, M. Osada, B. Y. Wang, D. Li, H. Y. Hwang, R. Pentcheva, and L. F. Kourkoutis, Resolving the polar interface of infinite-layer nickelate thin films, *Nat. Mater.* **22**, 466 (2023).
- [48] W. Kohn and L. J. Sham, Self-consistent equations including exchange and correlation effects, *Phys. Rev.* **140**, A1133 (1965).
- [49] P. Giannozzi, S. Baroni, N. Bonini, M. Calandra, R. Car, C. Cavazzoni, D. Ceresoli, G. L. Chiarotti, M. Cococcioni, I. Dabo, A. Dal Corso, S. de Gironcoli, S. Fabris, G. Fratesi, R. Gebauer, U. Gerstmann, C. Gougoussis, A. Kokalj, M. Lazzeri, L. Martin-Samos, N. Marzari, F. Mauri, R. Mazzarello, S. Paolini, A. Pasquarello, L. Paulatto, C. Sbraccia, S. Scandolo, G. Sclauzero, A. P. Seitsonen, A. Smogunov, P. Umari, and R. M. Wentzcovitch, QUANTUM ESPRESSO: a modular and open-source software project for quantum simulations of materials, *J. Phys.: Condens. Matter* **21**, 395502 (2009).
- [50] J. P. Perdew, K. Burke, and M. Ernzerhof, Generalized gradient approximation made simple, *Phys. Rev. Lett.* **77**, 3865 (1996).
- [51] D. Vanderbilt, Soft self-consistent pseudopotentials in a generalized eigenvalue formalism, *Phys. Rev. B* **41**, 7892 (1990).
- [52] B. Geisler and R. Pentcheva, Confinement- and strain-induced enhancement of thermoelectric properties in LaNiO₃/LaAlO₃(001) superlattices, *Phys. Rev. Materials* **2**, 055403 (2018).
- [53] F. Wrobel, B. Geisler, Y. Wang, G. Christiani, G. Logvenov, M. Bluschke, E. Schierle, P. A. van Aken, B. Keimer, R. Pentcheva, and E. Benckiser, Digital modulation of the nickel valence state in a cuprate-nickelate heterostructure, *Phys. Rev. Materials* **2**, 035001 (2018).
- [54] B. Geisler and R. Pentcheva, Inducing n - and p -type thermoelectricity in oxide superlattices by strain tuning of orbital-selective transport resonances, *Phys. Rev. Applied* **11**, 044047 (2019).
- [55] M. Cococcioni and S. de Gironcoli, Linear response approach to the calculation of the effective interaction parameters in the LDA+ U method, *Phys. Rev. B* **71**, 035105 (2005).
- [56] B. Geisler and R. Pentcheva, Fundamental difference in the electronic reconstruction of infinite-layer versus perovskite neodymium nickelate films on SrTiO₃(001), *Phys. Rev. B* **102**, 020502(R) (2020).
- [57] B. Geisler and R. Pentcheva, Correlated interface electron gas in infinite-layer nickelate versus cuprate films on SrTiO₃(001), *Phys. Rev. Research* **3**, 013261 (2021).
- [58] B. Geisler, S. Follmann, and R. Pentcheva, Oxygen vacancy formation and electronic reconstruction in strained LaNiO₃ and LaNiO₃/LaAlO₃ superlattices, *Phys. Rev. B* **106**, 155139

- (2022).
- [59] H. J. Monkhorst and J. D. Pack, Special points for Brillouin-zone integrations, *Phys. Rev. B* **13**, 5188 (1976).
- [60] M. Methfessel and A. T. Paxton, High-precision sampling for Brillouin-zone integration in metals, *Phys. Rev. B* **40**, 3616 (1989).
- [61] G. Pizzi, V. Vitale, R. Arita, S. Blügel, F. Freimuth, G. Géranton, M. Gibertini, D. Gresch, C. Johnson, T. Koretsune, J. Ibanez-Azpiroz, H. Lee, J.-M. Lihm, D. Marchand, A. Marrazzo, Y. Mokrousov, J. I. Mustafa, Y. Nohara, Y. Nomura, L. Paulatto, S. Poncé, T. Ponweiser, J. Qiao, F. Thöle, S. S. Tsirkin, M. Wierzbowska, N. Marzari, D. Vanderbilt, I. Souza, A. A. Mostofi, and J. R. Yates, Wannier90 as a community code: new features and applications, *J. Phys.: Condens. Matter* **32**, 165902 (2020).
- [62] See Supplemental Material at [URL will be inserted by publisher] for [give brief description of material].
- [63] Y. Zhang, L.-F. Lin, W. Hu, A. Moreo, S. Dong, and E. Dagotto, Similarities and differences between nickelate and cuprate films grown on a SrTiO_3 substrate, *Phys. Rev. B* **102**, 195117 (2020).
- [64] B. Geisler, Rashba spin-orbit coupling in infinite-layer nickelate films on $\text{SrTiO}_3(001)$ and $\text{KTaO}_3(001)$, *Phys. Rev. B* **108**, 224502 (2023).
- [65] B. Geisler, A. Blanca-Romero, and R. Pentcheva, Design of n - and p -type oxide thermoelectrics in $\text{LaNiO}_3/\text{SrTiO}_3(001)$ superlattices exploiting interface polarity, *Phys. Rev. B* **95**, 125301 (2017).
- [66] Z. Zhang, S. Soltan, H. Schmid, H.-U. Habermeier, B. Keimer, and U. Kaiser, Revealing the atomic and electronic structure of a $\text{SrTiO}_3/\text{LaNiO}_3/\text{SrTiO}_3$ heterostructure interface, *J. Appl. Phys.* **115**, 103519 (2014).
- [67] J. Hwang, J. Son, J. Y. Zhang, A. Janotti, C. G. Van de Walle, and S. Stemmer, Structural origins of the properties of rare earth nickelate superlattices, *Phys. Rev. B* **87**, 060101 (2013).